Climatic Change
DOI 10.1007/s10584-015-1520-1

Coastal sea level changes, observed and projected during the 20th and 21st century

M. Carson[1] · A. Köhl[1] · D. Stammer[1] · A. B. A. Slangen[2] · C. A. Katsman[3] · R. S. W. van de Wal[4] · J. Church[2] · N. White[2]

Received: 5 December 2014 / Accepted: 22 September 2015

Abstract Timeseries of observed and projected sea level changes for the 20th and 21st century are analyzed at various coastal locations around the world that are vulnerable to climate change. Observed time series are from tide gauges and altimetry, as well as from reconstructions over the last 50 years. CMIP5 coupled atmosphere-ocean model output of regional sea-level and associated uncertainty estimates are merged with scenario-independent contributions from GIA and dynamic ice to provide time series of coastal sea-level projections to the end of the 21st century. We focus on better quantifying the regional departure of coastal sea level rise from its global average, identify the reasons for the regional departure, and quantify the reasons for the uncertainty in these regional projections. Many of these coastal sea level projections are lower than the global mean change in sea level due to glacial isostatic adjustment, and gravitational changes from loss of land ice and terrestrially stored ground water. In most coastal regions, local deviations from the global mean vary up to ±20 cm which, depending on the location, differ substantially in their underlying causes.

Electronic supplementary material The online version of this article (doi:10.1007/s10584-015-1520-1) contains supplementary material, which is available to authorized users.

✉ M. Carson
mark.carson@uni-hamburg.de

[1] Center für Erdsystemforschung und Nachhaltigkeit (CEN), University of Hamburg, Bundesstrasse 53, Hamburg, 20146, Germany

[2] CSIRO Oceans and Atmosphere Flagship, GPO Box 1538, Hobart, TAS 7001, Australia

[3] Department of Hydraulic Engineering, TU Delft, Postbus 5, 2600 AA Delft, The Netherlands

[4] Institute for Marine and Atmospheric Research Utrecht (IMAU), Utrecht University, Princetonplein 5, 3584 CC Utrecht, The Netherlands

Published online: 14 October 2015

1 Introduction

Regional sea level changes deviate substantially from a global mean value. Underlying processes include dynamical ocean response and currents (Gregory et al. 2001; Yin et al. 2010; Stammer et al. 2013), static gravitational effects resulting from glacier and land ice mass changes (also known as 'fingerprints'; Mitrovica et al. 2001), terrestrial water storage changes (Wada et al. 2012), and Glacial Isostatic Adjustment (GIA; Peltier 2004). To a lesser extent, they also result from changes in the atmospheric pressure loading associated with changes in atmospheric circulation and in atmospheric moisture content (Wunsch and Stammer 1997; Stammer and Hüttemann 2008).

The focus of this study is relative sea level changes (i.e., relative to the solid earth's surface, henceforth RSL) in coastal regions around the world. The goal is to quantify to what extent these coastal RSL change estimates deviate from a global mean value and to highlight which process in particular is important as a function of geographic location. Various characteristic locations around the world are chosen which represent high population densities or highly vulnerable regions as identified by Nicholls and Cazenave (2010). Perrette et al. (2013) have previously explored RSL projections along coasts using patterns found in CMIP3 (plus glacier and land ice patterns) and scaled with CMIP5 global temperature, whereas here we have applied the newest set of model projections from CMIP5 and estimates of land ice and glacier contributions from Slangen et al. (2014). A similar approach to projecting regional sea level change was used in the IPCC AR5 (Church et al. 2013a) using different ice estimates. However, here we focus particularly on RSL projections at the coasts with an aim to understand the limitations of applying global climate models results to coasts in a simple way, and to more clearly understand the reasons why the rates of coastal sea level differ around the world and the uncertainty in these regional departures from the global average rise.

We analyze local sea level changes as observed over the last 50 years by tide gauge data and altimetry and compare them with projections obtained from an ensemble of 21 CMIP5 climate models simulating sea level change through 2100. In addition to these multi-model ensemble-mean regional climate projections, various other contributions to RSL changes are considered (Slangen et al. 2014). Notably, the estimate combines CMIP5 dynamical and global mean thermosteric sea level projections of the coupled climate system with regional estimates of additional static responses due to changes in land ice, groundwater, and the solid earth response.

2 Methodology

Regional RSL change projections for the end of the twenty-first century are provided recently by Slangen et al. (2014) based on the latest atmosphere-ocean general climate model (AOGCM) simulations assembled in the WRCP Fifth Coupled Model Intercomparison Project (CMIP5; Taylor et al. 2012). An ensemble of 21 AOGCM projections was analyzed, using the Representative Concentration Pathways (RCP; Moss et al. 2010) 4.5 and 8.5 scenarios, to assess the impacts of a moderate mitigation and a non-mitigation climate change scenario. All data are shown on a common $1^\circ \times 1^\circ$ grid. These regional projections were combined with model-based projections and observation-based estimates of land ice (Slangen et al. 2012; Meehl et al. 2007; Katsman et al. 2011), groundwater depletion (Wada et al. 2012) and GIA (Peltier 2004) to provide total regional change estimates, and their spatial fingerprints. For details on these components, and their estimated uncertainties,

see Slangen et al. (2014). For the rest of the paper, RSL change refers to regional sea level change relative to the solid earth's surface, and includes the global mean thermosteric sea level change.

For the analysis of present-day RSL changes, we use satellite altimetry data compiled and gridded by CSIRO Oceans and Atmosphere Flagship, tide gauges from the Permanent Service for Mean Sea Level (Holgate et al. 2013; PSMSL 2012), and an updated CSIRO historical sea level recontruction based on the methods in Church et al. (2004) (hereafter referred to as CW09). The CW09 and altimetry data both contain the global mean sea-level change signal, and have not been corrected for GIA uplift, and as such effectively describe sea level relative to a time-mean geoid. All data, instrumental and modeled, have been averaged into annual means to focus on the long-term sea level changes, including interannual and interdecadal variability. Gaps in monthly PSMSL tide gauge data are filled before averaging into annual means by fitting the gap with the monthly climatology added to the instantaneous 'trend' between the last point before and first point after the gap. For nearly all tide gauge data used, this has very little effect on the annual means, and only fills gaps of a year or longer for three tide gauges.

For the analyses in Section 3, coastal-only locations were found by selecting those grid cells on the $1^\circ \times 1^\circ$ grid where at least one side bordered a land cell (i.e., a masked grid box). This yields 2932 coastal grid boxes for this grid.

The data used to provide figures are available, as explained in the Acknowledgments.

3 Results

3.1 Projected RSL changes

When the various contributions to regional sea level are summed together, the projected RSL patterns, 2081–2100 minus 1986–2005, contain considerable spatial variations (Fig. 1). These variations are partly from the dynamic height contributions, but also from a local fall in sea level near the ice sheets, as well as additional changes resulting from GIA in the Scandinavian, Russian and Canadian Arctic regions (Perrette et al. 2013; Slangen et al. 2014), and groundwater. Patterns related to ice sheet loss result from lowered gravitational attraction in the vicinity of ice mass loss in the Arctic, Greenland and Western Antarctica, and a larger than global average remote rise at middle and low latitudes as mass flows away from the ice sheets in response to the lowered gravitational attraction. The regional sea level for the 2081–2100 mean is significantly different, using the t-test, from the 1986–2005 mean for about 95 % of the world ocean at the 90 % level, with respect to the regional uncertainty estimates in all components (see Slangen et al. (2014) for details on uncertainty estimation and sea-level change values) for both RCP4.5 and 8.5 scenarios. This large-scale field significance is mostly due to the global thermosteric signal, whose uncertainty contributes to only a portion of the regional uncertainty, and to the ice mass loss signal, which has a large-scale regional pattern. Only Arctic regions and regions around Greenland and western Antarctica undergo RSL change significantly different from the global mean, where the substantial ice uncertainties have their largest regional impact, in addition to a small net local RSL change (Slangen et al. 2014).

Coastal sea level statistics are compared with global statistics to highlight similarities and differences. Even though the coastal distributions are highly skewed (Fig. 2), over 80 % of the coastal values lie within 20 cm of the global mean. The negative deviation of the coastal mean is caused essentially through the gravitational drop in sea level around declining ice

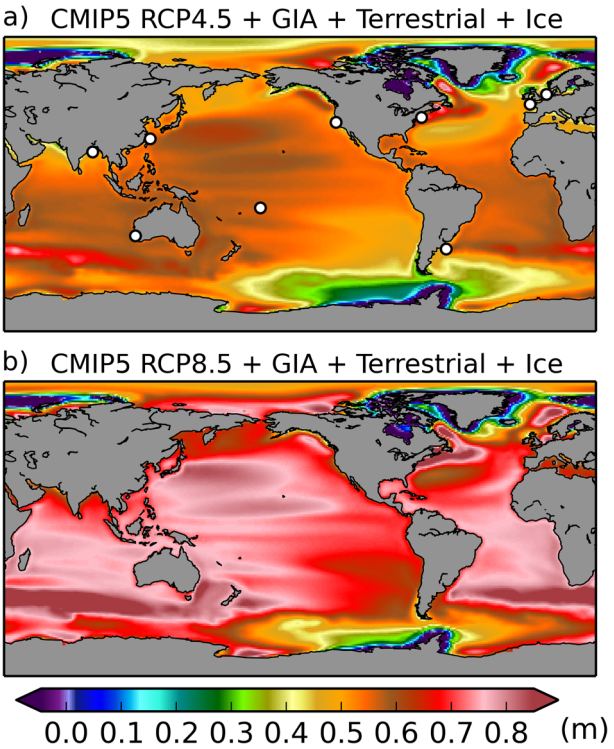

Fig. 1 Regional sea-level change patterns of sea-level contributions. **a** Projected regional sea-level change patterns from RCP4.5 including the global mean over the period from 1986–2005 to 2081–2100, in m. The field is constructed from the ensemble mean (21 AOGCMs) CMIP5-RCP4.5 glacier, global thermosteric expansion, atmospheric loading, ice sheet, groundwater and GIA contributions (Slangen et al. 2014). The *white dots* indicate the location of stations shown in Fig. 3. **b** The same as for panel (**a**) but for RCP8.5. Note the similiarity of the spatial pattern

sheets and glaciers, especially large around western Antarctica and Greenland, leading to negative sea level changes; i.e., a drop in sea level relative to present conditions, which results in a skewed distribution function. The higher side of the distribution is caused largely by increased sea level rise in the far field from the ice loss gravitational pattern (see Fig. 2 Slangen et al. 2014), but also due in particular regions to positive changes in dynamic SSH. In some regions, GIA plays a large role in land subsidence by the decrease in the forebulge from the last glacial maximum. The highly skewed coastal distribution yields a coastal mean RSL change for RCP4.5 of 42.4 cm (global mean is 53.5 cm); for RCP8.5, the coastal mean change is 57.8 cm (global mean is 71 cm). The coastal mean is lower because the largest RSL change values mostly lie in the open ocean away from most coastlines, as can be seen in Fig. 1. There are many small islands in the central Pacific, where large changes in RSL are projected to be; these islands and their coasts are not resolved on this grid.

Shown in Fig. 3 are observed and projected sea level changes for individual coastal stations as indicated by white dots in Fig. 1a. Locations were selected according to their societal relevance but also to the availability of long tide gauge time series. In most locations, observations reveal the presence of strong internnual to decadal variability. Internal

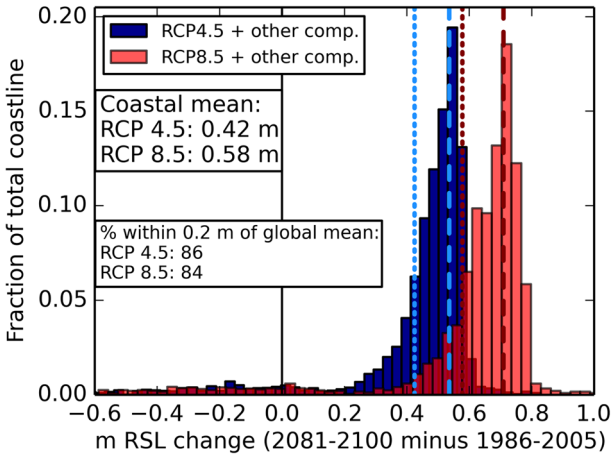

Fig. 2 Coastal RSL change distributions. Relative sea-level change distributions only along coastlines for the RCP4.5 and RCP8.5 scenarios between 2081–2100 and 1986–2005, in m along the x-axis, and the fraction of total coastline distance along the y-axis (for the ensemble results on a 1 × 1 grid). The *dashed line* shows the global mean value of RSL change for the scenario; the *dotted line* shows the coastal mean RSL. Most of the coastal changes in sea level lie within 0.2 m of the global mean. The root-mean-square deviation of RCP4.5 coastal changes relative to the global mean is 28.8 cm, for RCP8.5 it's 34.4 cm. Given the skewness, the weighted medians (weighted for grid box sizes) for the coastal and global values lie closer together: for RCP4.5, the coastal and global medians are 50 and 56 cm; for RCP8.5, the coastal and global medians are 68 and 74 cm, respectively

variability is also present in individual model time series, as shown for 3 single models, but is mostly averaged out in the ensemble mean. These individual model time series have the same ice estimate added for the same location, and the uncertainty shown by the grey envelope is due to the combined uncertainties from all components (Slangen et al. 2014). Although the altimetry time series are very short relative to the tide gauge records and the projections, there is no obvious disagreement between the slopes of the time series where they coincide. A change in slope for the San Francisco tide gauge involves decadal variability in local sea level (Zhang and Church 2012); in fact, the tide gauge trend over the last 20 years is slightly negative, whereas the 1970-to-present trend is positive. It is not yet clear how well model variability reproduces the magnitude and phase of real-world local RSL variability on longer time scales.

The figure clearly shows regional differences in the amount of future sea level changes. As also shown in Fig. 1, the highest anticipated coastal increase is in the northwestern North Atlantic, leading to a potential RSL increase of up to 80 ± 40 cm (for RCP8.5) in the vicinity of New York (Slangen et al. 2012). This sea level increase in model data has been analyzed by Yin et al. (2009) and Sallenger et al. (2012); it is the result of climate-forced circulation changes, though on the broader regional scale, direct fluxes of heat and freshwater are also important (Bouttes et al. 2014). In addition to the climate model data, the GIA impact on sea level in this region is also expected to be very high, and contributes over half of this signal (see the section on RSL Components below). The figure also shows the spatial inhomogeneity of the uncertainties, i.e., the size of the grey envelopes, in the projections.

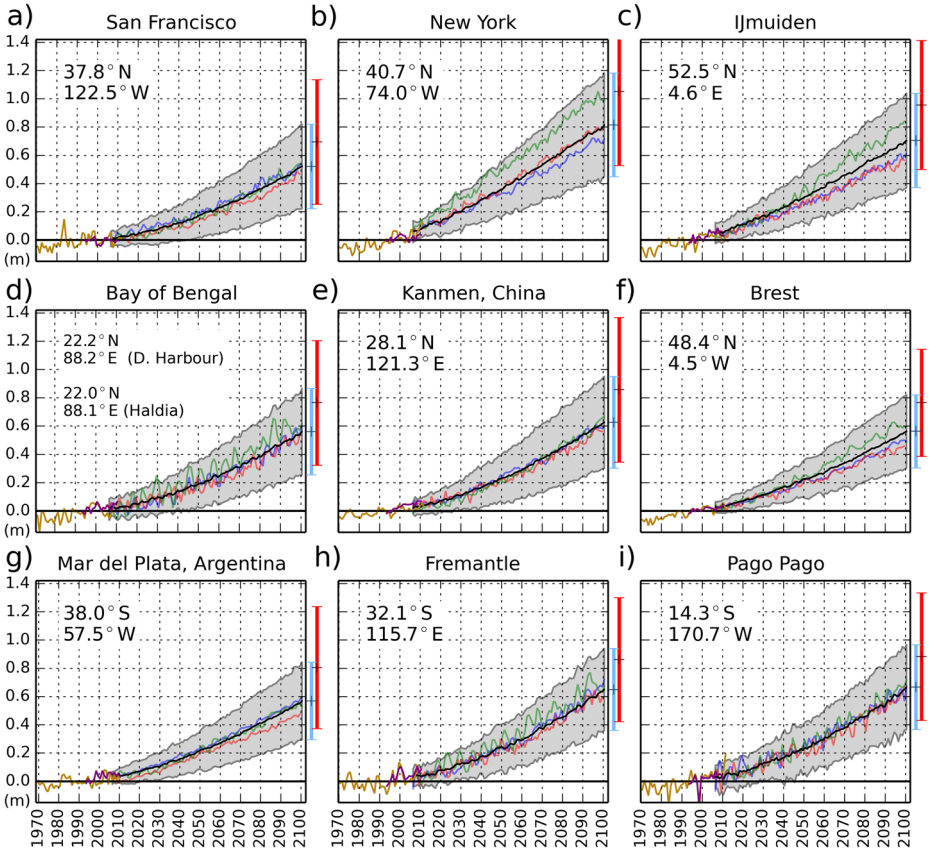

Fig. 3 Individual coastal stations. Observed and projected relative sea level change near nine representative coastal locations for which long-term tide-gauge measurements are also available. The observed in situ sea-level from tide gauges (since 1970) is plotted in *yellow*, and the satellite record (since 1993) in *purple*. The projected range from 21 CMIP5 RCP 4.5 scenario runs plus other components (from their combined 90 % uncertainty estimate) is shown by the shaded region for the period 2006–2100; the *black line* is the ensemble mean. *Colored lines* represent individual AOGCM realizations drawn randomly from three different AOGCMs (plus other components) to highlight temporal variability. All time series are anomalies relative to their 1986–2005 mean value (1993–1997 mean value for altimetry). Station locations of the tide gauges are inset; Bay of Bengal is the average of two tide gauges. *Vertical bars* at the right sides represent the ensemble mean and spread of sea level change at each location in year 2100 for the RCP 4.5 (*light blue*) and 8.5 (*red*). Note that the RCP8.5 errorbar for New York extends to 1.58 m

3.2 Time scales of emergence

When comparing AOGCM projections with observed sea level time series containing natural variability, a useful question to ask is: at a particular location, what is the time interval required before the measured trend passes a 90 % CL t-test in the model data? These time intervals are shown in Fig. 4 based on trends of the ocean-only regional model data (including the global thermosteric signal) starting at the beginning year of the RCP scenarios, 2006. First, the degrees of freedom for the time series are reduced by the model historical data's integral time scales from the period 1950–2006, that is, the autocorrelation function is calculated from the model dynamic SSH data, and the time scale from the integration of

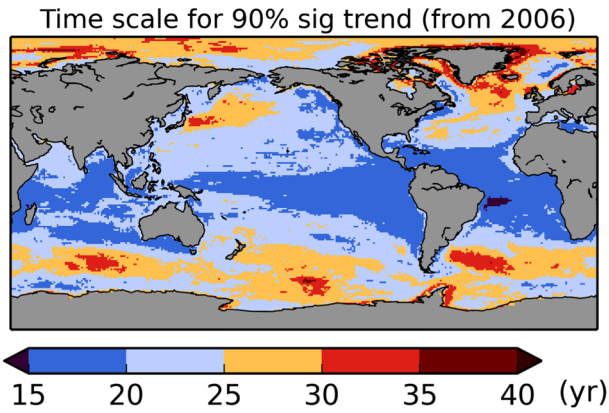

Fig. 4 Time scales of emerging regional sea level. Time interval required before the measured trend passes a 90 % CL test. The degrees of freedom are adjusted by the historical data's integral time scale, which therefore tests against model internal variability. Shown is the ensemble average of the time intervals, which are calculated on per-model basis. Analyzed time series' intervals all start from 2006 for the full regional RSL change projection, the difference change of which is shown in Fig. 1

the function to the first zero-crosing is estimated (see section 3.15.1, Emery and Thomson 2004). This integral time scale therefore provides an estimate of model internal variability. The forced, historical model data is used instead of control run data in order to account for possible modulation of the model's internal climate variability in a changing climate. Then, ordinary least-squares trends are estimated and tested for 90 % CL significance in a sequence of increasing time intervals (e.g., 2006–2016, 2006–2021, 2006–2026, etc.) with respect to the null hypothesis of zero trend. At the point where the time series is long enough to continue to pass the 90 % CL test for all longer time frames, this is recorded as the 'time of emergence' for that model. The needed detection time arises from a combination of the strength of the local sea level trend and the amount of internal climate variability at that location. Figure 4 shows the ensemble mean of these minimum time frames from all the models. The figure reveals that, over extensive parts of the ocean, time series of more than 20 years in duration are required before a significant trend can be estimated. In western boundary current regions, along the Antarctic Circumpolar Current and in the Arctic, the needed monitoring period actually exceed 30 years. Only in some tropical or subtropical regions is the long-term signal detectable in shorter than 20 years. It should be noted that the internal variability in the real ocean is likely different than that estimated here, as discussed below, and this may require the needed monitoring period to detect trends be different in some regions.

Tide gauge data were also used to estimate the time scale of measurement needed to detect significant RSL trends at individual locations in a similar fashion, and are compared to the model results (Table 1). For the tide gauges available with sufficiently long records, the period chosen for analysis is usually 1962–2011 (inclusive), though some of the gauges chosen have no data after 2010 or 2008, and so the period analyzed is the last 50 years to the end of the record (data from PSMSL as of early 2012). The autocorrelation function for each tide gauge is calculated along the same time frame to provide the integral time scale for the reduction of the degrees of freedom. Finally, trends are calculated for all time frames starting from 50 years in length backwards (50 yrs, 49 yrs, etc.) and tested for 90 % CL t-test significance of being different than zero slope. The time frame for which the trend first passes the 90 % CL test, and continues to pass for all longer time frames, is marked

Table 1 **(columns 2 and 3)** Time, in yrs from the starting year indicated, until the sea level trend line passes 90 % CL significance test (trend different from zero) for all longer time intervals

Location	Tide gauge from 1962[a]	Model ensemble from 2006	TG-model trend ratio	TG-model stddev ratio
IJmuiden, Netherlands	37	23	0.4	1.2
New York City	23	19	0.4	1.4
San Francisco, CA	31	21	0.5	2.3
Brest, France	34	21	0.4	1.6
Kanmen, China	21	22	0.7	1.1
Bay of Bengal †	15	21	3.5	1.9
Pago Pago	38	21	0.4	1.3
Fremantle, Australia ‡	48	21	0.3	1.7
Mar del Plata, Argentina ‡	47	24	0.2	2.2

For tide gauges, the starting year has a few exceptions, as some tide gauges are missing a few years' data towards the end of the record (e.g., the data run from 1959 to 2008 for Bay of Bengal, Diamond Harbour). The model trends are all tested from the starting year 2006. The model ensemble value is the ensemble mean shown in Fig. 4b. **(column 4)** Ratio of the trend magnitude of the tide gauge record vs. the model data over the time interval shown in columns 2 and 3, respectively. These trends also start from the same respective starting points. **(column 5)** Ratio of the standard deviation of the detrended tide gauge time series vs. the detrended model data over the same respective time intervals.

[a]Exceptions are marked. †: from 1959; ‡: from 1961

as the time of emergence. These numbers are shown in Table 1 for selected coastal cities and compared to the ensemble mean of the time scale of emergence shown in Fig. 4. The tide gauges mostly exhibit a longer time scale of significant RSL trend detection than the models. This is mostly due to the weaker trend of the tide gauges over the earlier period (column 4), and also partially because of the different magnitude of internal variability in the tide gauge data as compared to the projected model data (column 5). The Bay of Bengal tide gauge at Diamond Harbor is an anomaly here, since this time series during the 1960s exhibits a steep increase in RSL (not shown in Fig. 3). Richter and Marzeion (2014) also find that the time period required to detect significant trends (the time of local emergence) is longer prior to the satellite era, though this was within model results alone. It is certainly worth noting that in all tide gauges shown, the RSL change signal is already statistically detectable. On a related note, it may be possible from now on (assuming continuing global climate monitoring) that the internal variability signal can be estimated and removed from the total to allow estimation of the secular RSL change (Cazenave et al. 2014). Regional sea-level rise emergence time scale results for projected RSL changes have also been estimated in more detail by Lyu et al. (2014) and Richter and Marzeion (2014), who find results of similar magnitude to the ones shown here in Fig. 4. Another study by Jordà (2014) found time scales which were longer than those reported here by 15 or more years, depending on the strength of the regional trend.

3.3 RSL components

Breaking down local sea-level change by component in RCP4.5 (Fig. 5), the ocean component and the various ice sources (when added together) are the two largest sources of RSL change. The ocean component here includes the global thermosteric signal, which is the

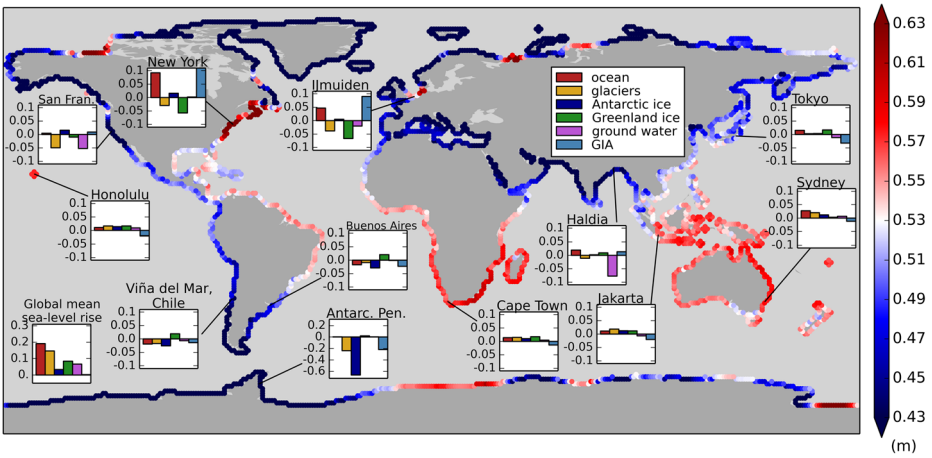

Fig. 5 Coastal sea level: relative to global mean, and by component. RCP4.5 plus other components: coastal values of mean relative sea level (RSL) rise in 2081–2100, in m, with the central value of the colorbar being the global mean RSL rise. Therefore, redder regions correspond to coasts projected to have higher RSL rise, and bluer regions to have less RSL rise, than the global average. Inset boxes show a set of selected locations along with the size of the contributions to RSL change at that location, with zero being the global mean for that component, in m. Contains RCP4.5 model results plus scenario-independent contributions. Note that the GIA anomaly for New York extends to 0.18. The pattern for RCP 8.5 is not shown here, but is similar in its regional pattern, though with higher magnitudes of RSL change (both positive and negative). The stations were selected in this figure to cover diverse coastal locations with large population centers, with the exception of the Antarctic Peninsula

largest part at 0.19 m for RCP4.5 and 0.27 m for RCP8.5, dynamic SSH changes which are robust in the ensemble mean, and the inverse barometer effect (which is always small: less than 0.05 m, regionally). For ice, glaciers have the largest impact nearly everywhere (and in the global mean), but whether the Greenland or Antarctic ice sheets dominate the local RSL is dependent on the location. The imprint of the spatial pattern of RSL from the ice sheet melt can be seen in Fig. 5 in the yellow, dark blue and green bars. The closer the location is to the center of land-ice loss, the lower the RSL signal is from this component, since the gravitational attraction to the reduced land ice mass is smaller (e.g., New York and IJmuiden, which are close to the centers of mass loss for Greenland ice and the glaciers, which lie across northern Canada and the Arctic islands in this analysis), and the RSL change is larger far away from these locations (e.g., Sydney and Tokyo). The same goes for the Antarctic ice signal, with Buenos Aires and Viña del Mar having low RSL change from this component, and Northern Hemisphere locations having higher RSL change. Haldia and San Francisco have lower ground water sea-level contributions, being near centers of ground water reservoir loss, with most other regions having higher ground water contributions. Finally, the ocean RSL component reflects, in part, the dynamic SSH change pattern from circulation changes, the rest being the global average thermosteric signal. Note that the most impacted regions for higher RSL due to ice and ground water loss include much of the western tropical Pacific, which exacerbates the problem of rising sea level for many of the small islands there, and the eastern tropical Indian ocean for cities with vulnerable coasts (Cazenave and Le Cozannet 2013). The highest positive coastal RSL change relative to the global mean in populated regions occurs along the northeast coast of North America, which is a highly

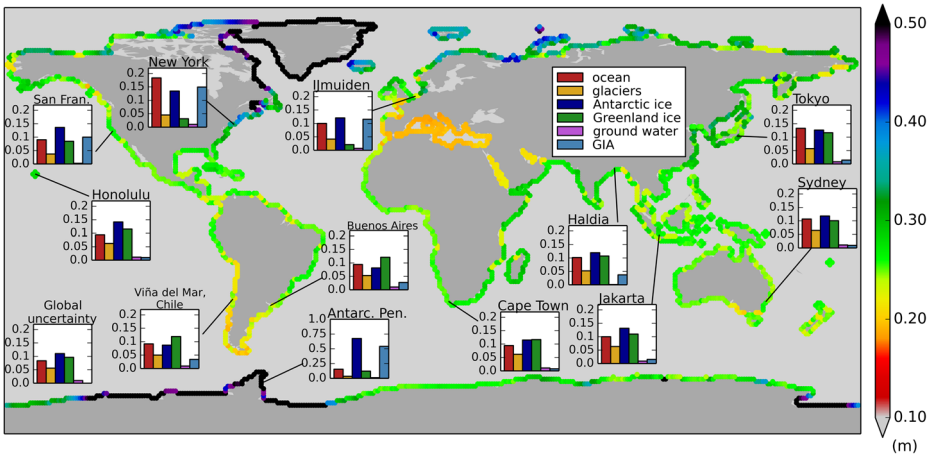

Fig. 6 Coastal sea level uncertainty: global and by component. Shown is the 90 % one-sided uncertainty, in m, by component for the RCP4.5 scenario, plus other scenario-independent components. The vertical scale of the insets is the same as in Fig. 5, as are the locations. The coastal values corresponding to the colorbar are the total uncertainty for RSL from all component uncertainties combined (uncertainties were combined as described in Church et al. 2013b). An important detail to note is that the large regional uncertainties for the ice are directly related to the global ice uncertainty. So a change in a global ice value is reflected in the pattern of the sea level change for that ice component

populated coastline, including New York City. For spatial maps of these patterns, see Slangen et al. (2014), Fig. 1, or Church et al. (2013a), Fig. 13.18.

The 90 % one-sided uncertainties for the RCP4.5 scenario are shown in Fig. 6. A comparison of the local RSL component uncertainties (the insets) to the component anomaly values of Fig. 5 reveals that the local component RSL changes do not lie outside of their uncertainties relative to the global mean component values for nearly all populated coastal regions. Most contributions to regional RSL change are either large-scale patterns that scale with the global mean value of that component, as for ice mass loss, or are contributions for which the whole field sums globally to zero, as for the model dynamic sea surface height (which by definition has zero global mean) and atmospheric loading (Slangen et al. 2014). GIA also sums nearly to zero in the global mean, which means that most local changes in one location are compensated in another (Peltier 2004). Thus, even though the RSL change of individual locations are within the uncertainty limits of the global mean, the existence of a regional pattern of RSL change differing from the global mean is certain. The same holds for the uncertainties. For instance, the ice uncertainties for certain regions, such as in the Indian and Pacific tropical regions and for Cape Town, are bigger than for the global ice uncertainty, and this again emphasizes that the local impact of RSL change in these regions is strongly related to the projected amount of land ice loss.

4 Concluding remarks and outlook

We investigated observed and projected sea level changes to better quantify the departure of coastal sea level rise from the global average. Over 80 % of local sea-level projections differ from the projected global mean by up to ±20 cm, even though most of the populated coastal

region projections are not statistically different from the global mean. Such differences can be important to unprotected coastlines, especially when coupled with storm surges, land subsidence from ground water extraction, and erosion. Kopp et al. (2014) also reported on coastal sea level change magnitudes at tide gauge locations, finding substantial increases in flood risk for future projections of sea-level rise. In our analysis, New York City and the populated coastline of northeast North America are projected to undergo the largest change in RSL of any densely populated region. It is vital to take the results presented here, based on AOGCMs, as a background for the coastal sea-level change at any specific location, which requires an improved estimate that incorporates vertical land motion and erosion processes. Only then can vulnerability estimates be made, based on the projected physical parameters coupled with the local socio-economic situation and topographic conditions (Nicholls 2011). The vertical land motion estimates are in need of improvement, and these efforts continue (e.g., Santamaría-Gómez et al. 2014). In addition to land subsidence from groundwater extraction and GIA, regions with high tectonic activity (Ballu et al. 2011) and coastal wetlands (Cahoon 2015) are places where vertical land motion needs to be accounted for.

The size of the land ice component contributions presented here are the same as those presented in Slangen et al. (2014), and are nearly the same magnitude as those presented in the IPCC-AR5. The Slangen et al. (2014) estimate is a single estimate, whereas the IPCC-AR5 estimate is an assessment of many available studies using various techniques, though these two estimates are within their respective uncertainties from each other. The land ice contributions to sea level rise estimated using semi-empirical methods in Perrette et al. (2013) are larger, and drive local RSL changes to nearly a meter in many coastal locations (see, e.g., their Figs. 8 through 11, and in particular New York). However, semi-empirical methods tend to estimate larger ice mass loss projections than do process-based methods (Church et al. 2013a). Even so, a possible collapse of the West Antarctic Ice Sheet could contribute additional sea-level rise, though the probability of this is difficult to constrain (Church et al. 2013a).

Ultimately, thermal expansion and land ice changes contribute the most to projections of future sea level rise, with land ice changes possibly being a larger source, due to the large error bars on the ice loss estimates. Sea level rise from land ice loss over the next 100 years, regardless of global magnitude, will be enhanced in middle to low latitudes where the bulk of the coastal human population resides. The variations over these coastal regions are not particularly large, on average ranging between 10 and 20 cm, though there are specific regions which may undergo much different RSL change than the global mean, due to projected thermosteric expansion (New York), GIA changes (Stockholm, New York and IJmuiden), or continued subsidence from ground water extraction, as for Manila (see Online Resource on present-day RSL).

The global climate results presented here provide the groundwork for future coastal impact and vulnerability studies, which can be improved with with necessary local modifications due to vertical land motion, erosion and other processes which are not modeled here. Regional modeling, using the open ocean values from the climate models as a boundary condition, can also provide improved estimates for impact studies.

Acknowledgments This work was funded in part through CliSAP Excellence Cluster of the University of Hamburg, funded through the DFG, the BMBF (Federal Ministry of Education and Science) Project RACE, and a Max Planck Society(MPG) Fellowship to D. Stammer. ABA Slangen was funded by NWO and KvK. The data are available from icdc.zmaw.de under Coastal Sea Level.

References

Ballu V, Bouin M, Siméoni P, Crawford WC, Calmant S, Boré J, Kanas T, Pelletier B (2011) Comparing the role of absolute sea-level rise and vertical tectonic motions in coastal flooding, Torres Islands (Vanuatu). Proc Natl Acad Sci USA 108(32):13019–13022. doi:10.1073/pnas.1102842108

Bouttes N, Gregory JM, Kuhlbrodt T, Smith RS (2014) The drivers of projected North Atlantic sea level change. Clim Dyn 43(5–6):1531–1544. doi:10.1007/s00382-013-1973-8

Cahoon DR (2015) Estimating relative sea-level rise and submergence potential at a coastal wetland. Estuar Coasts 38:1077–1084. doi:10.1007/s12237-014-9872-8

Cazenave A, Le Cozannet G (2013) Sea level rise and its coastal impacts. Earth's Future 2:15–34. doi:10.1002/2013EF000188

Cazenave A, Dieng HB, Meyssignac B, von Schuckmann K, Decharme B, Berthier E (2014) The rate of sea-level rise. Nat Clim Change 4:358–361. doi:10.1038/nclimate2159

Church JA, White NJ, Coleman R, Lambeck K, Mitrovica JX (2004) Estimates of the regional distribution of sea-level rise over the 1950 to 2000 period. J Clim 17:2609–2625

Church JA, Clark P, Cazenave A, Gregory J, Jevrejeva S, Levermann A, Merrifield M, Milne G, RSNerem NunnP, Payne A, Pfeffer W, Stammer D, Unnikrishnan A (2013a) Sea level change. In: Stocker TF, Qin D, Plattner GK, Tignor M, Allen S, Boschung J, Nauels A, Xia Y, Bex V, Midgley P (eds) Climate change 2013: the physical science basis. Cambridge University Press, Cambridge and New York

Church JA, Clark P, Cazenave A, Gregory J, Jevrejeva S, Levermann A, Merrifield M, Milne G, Nerem RS, Nunn P, Payne A, Pfeffer W, Stammer D, Unnikrishnan A (2013b) Sea level change supplementary material. In: Stocker TF, Qin D, Plattner GK, Tignor M, Allen S, Boschung J, Nauels A, Xia Y, Bex V, Midgley P (eds) Climate change 2013: the physical science basis, available from www.climatechange2013.organdwww.ipcc.ch

Emery WJ, Thomson RE (2004) Data analysis methods in physical oceanography. Elsevier, Amsterdam

Gregory JM, Church JA, Boer GJ, Dixon KW, Flato GM, Jackett DR, Lowe JA, O'Farrell SP, Roeckner E, Russell GL, Stouffer RJ, Winton M (2001) Comparison of results from several AOGCMs for global and regional sea-level change 1900–2100. Clim Dyn 18:225–240. doi:10.1007/s003820100180

Holgate SJ, Matthews A, Woodworth PL, Rickards LJ, Tamisiea ME, Bradshaw E, Foden PR, Gordon KM, Jevrejeva S, Pugh J (2013) New data systems and products at the Permanent Service for Mean Sea Level. J Coast Res 29:493–504. doi:10.2112/JCOASTRES-D-12-00175.1

Jordà G (2014) Detection time for global and regional sea level trends and accelerations. J Geophys Res Oceans 119:7164–7174. doi:10.1002/2014JC010005

Katsman CA, Sterl A, Beersma JJ, van den Brink HW, Church JA, Hazeleger W, Kopp RE, Kroon D, Kwadijk J, Lammersen R, Lowe J, Oppenheimer M, Plag HP, Ridley J, von Storch H, Vaughan DG, Vellinga P, Vermeersen LLA, van de Wal RSW, Weisse R (2011) Exploring high-end scenarios for local sea level rise to develop flood protection strategies for a low-lying delta—the Netherlands as an example. Clim Change 109:617–645. doi:10.1007/s10584-011-0037-5

Kopp RE, Horton RM, Little CM, Mitrovica JX, Oppenheimer M, Rasmussen DJ, Strauss BH, Tebaldi C (2014) Probabilistic 21st and 22nd century sea-level projections at a global network of tide-gauge sites. Earth's Future 2:383–406. doi:10.1002/2014EF000239

Lyu K, Zhang X, Church JA, Slangen ABA, Hu J (2014) Time of emergence for regional sea-level change. Nat Clim Change 4(11):1006–1010. doi:10.1038/nclimate2397

Meehl GA, Stocker TF, Collins WD, Friedlingstein P, Gaye A, Gregory J, Kitoh A, Knutti R, Murphy J, Noda A, Raper S, Watterson I, Weaver A, Zhao ZC (2007) Global climate projections. In: Solomon S, Qin D, Manning M, Chen Z, Marquis M, Averyt KB, Tignor M, Miller HL (eds) Climate change 2007: the physical science basis. Cambridge University Press, Cambridge and New York

Mitrovica JX, Tamisiea ME, Davis JL, Milne GA (2001) Recent mass balance of polar ice sheets inferred from patterns of global sea-level change. Nature 409:1026–1029

Moss RH, Edmonds JA, Hibbard KA, Manning MR, Rose SK, van Vuuren DP, Carter TR, Emori S, Kainuma M, Kram T, Meehl GA, Mitchell JFB, Nakicenovic N, Riahi K, Smith SJ, Stouffer RJ, Thomson AM, Weynant JP, Wilbanks TJ (2010) The next generation of scenarios for climate change research and assessment. Nature 463:747–756. doi:10.1038/nature08823

Nicholls RJ (2011) Planning for the impacts of sea level rise. Oceanography 24(2):144–157. doi:10.5670/oceanog.2011.34

Nicholls RJ, Cazenave A (2010) Sea-level rise and its impact on coastal zones. Science 328(5985):1517–1520. doi:10.1126/science.1185782

Peltier W (2004) Global glacial isostasy and the surface of the ice-age earth. Annu Rev Earth Planet Sci 32:111–149

Permanent Service for Mean Sea Level (PSMSL) (2012) Tide gauge data. Retrieved 7 Aug 2012 from www.psmsl.org/data/obtaining/

Perrette M, Landerer F, Riva R, Frieler K, Meinshausen M (2013) A scaling approach to project regional sea level rise and its uncertainties. Earth Syst Dyn 4:11–29. doi:10.5194/esd-4-11-2013

Richter K, Marzeion B (2014) Earliest local emergence of forced dynamic and steric sea-level trends in climate models. Environ Res Lett 9:114009. doi:10.1088/1748-9326/9/11/114009

Sallenger AH Jr, Doran KS, Howd PA (2012) Hotspot of accelerated sea-level rise on the Atlantic coast of North America. Nat Clim Change 2:884–888. doi:10.1038/nclimate1597

Santamaría-Gómez A, Gravelle M, Wöppelman G (2014) Long-term vertical land motion from double-differenced tide gauge and satellite altimetry data. J Geodyn 88:207–222. doi:10.1007/s00190-013-0677-5

Slangen ABA, Katsman CA, van de Wal RSW, Vermeersen LLA, Riva REM (2012) Towards regional projections of twenty-first century sea-level change based on IPCC SRES scenarios. Clim Dyn 38(5–6):1191–1209. doi:10.1007/s00382-011-1057

Slangen ABA, Carson M, Katsman CA, van de Wal RSW, Köhl A, Vermeersen LLA, Stammer D (2014) Projecting twenty-first century regional sea-level changes. Clim Change. doi:10.1007/s10584-014-1080-9

Stammer D, Hüttemann S (2008) Response of regional sea level to atmospheric pressure loading in a climate change scenario. J Clim 21:2093–2101. doi:10.1175/2007JCLI1803.1

Stammer D, Cazenave A, Ponte RM, Tamisiea ME (2013) Causes for contemporary regional sea level changes. Annu Rev Mar Sci 5:21–46. doi:10.1146/annurev-marine-121211-172406

Taylor KE, Stouffer RJ, Meehl GA (2012) An overview of CMIP5 and the experiment design. Bull Am Meteor Soc 93:485–498

Wada Y, van Beek LPH, Weiland FCS, Chao BF, Wu YH, Bierkens MFP (2012) Past and future contribution of global groundwater depletion to sea-level rise. Geophys Res Lett 39:L09402. doi:10.1029/2012GL051230

Wunsch C, Stammer D (1997) Atmospheric loading and the oceanic "inverted barometer" effect. Rev Geophys 35:79–107

Yin J, Schlesinger ME, Stouffer RJ (2009) Model projections of rapid sea-level rise on the northeast coast of the United States. Nat Geo 2:262–266. doi:10.1038/ngeo462

Yin J, Griffies SM, Stouffer RJ (2010) Spatial variability of sea-level rise in 21st century projections. J Clim 23:4585–4607

Zhang X, Church JA (2012) Sea level trends, interannual and decadal variability in the Pacific Ocean. Geophys Res Lett 39(L21701). doi:10.1029/2012GL053240